Dalton Transactions

ROYAL SOCIETY OF CHEMISTRY

PAPER

View Article Online
View Journal | View Issue

Cite this: *Dalton Trans.*, 2025, **54**, 9503

Synthesis, characterization and induction of ferroptosis of iridium(III) complexes against B16 melanoma cells†

Zhujun Sheng,[a] Yuanzheng Liu,[a] Li Xu,*[b] Xin Yao,[a] Ju Chen,[a] Yunjun Liu *[a] and Xiuzhen Wang*[a]

The synthesis of the ligand 2-(2-methyl-4-hydroxyl)phenyl-1*H*-imidazo[4,5-*f*][1,10]phenanthroline (MHIP) and its corresponding new iridium(III) complexes $[Ir(ppy)_2(MHIP)]PF_6$ (ppy = 2-phenylpyridine, **9a**), $[Ir(bzq)_2(MHIP)]PF_6$ (bzq = benzo[*h*]quinolone, **9b**) and $[Ir(piq)_2(MHIP)]PF_6$ (piq = 1-phenylisoquinoline, **9c**) was reported. The antiproliferative activity of compounds **9a–9c** on HepG2, B16, and A549 cancer cells as well as on normal NIH 3T3 cells was tested using a 3-(4,5-dimethylthiazol-2-yl)-2,5-diphenyltetrazolium bromide (MTT) assay. It was found that the three complexes showed moderate cytotoxicity in A549 and B16 cells. However, after further irradiation, the cytotoxicity was greatly enhanced; especially, **9a**, **9b** and **9c** displayed significant cytotoxicity toward B16 cells with a low IC_{50} value of 3.1 ± 0.3 μM for **9a**, 4.9 ± 0.8 μM for **9b**, and 0.4 ± 0.1 μM for **9c**. The effects of **9a–9c** on the invasive ability of B16 cells were explored *via* colony formation and scratch experiments. Results demonstrated that the complexes could efficiently block cell proliferation and migration. The co-localization assay found that **9a–9c** accumulated in the mitochondria and led to the apoptosis of B16 cells by decreasing mitochondrial membrane potential, altering the structure of microtubule proteins, damaging the structure of cellular DNA, and changing the expression of related proteins. The decrease in glutathione (GSH) concentration, the increase in malondialdehyde (MDA), the downregulation of GPX4, and C11-BODIPY staining results confirmed that **9a**, **9b** and **9c** led to ferroptosis. In addition, we explored the relevant signaling pathways through an RNA sequencing assay and speculated on the possible anticancer mechanisms. Together, the results of this study indicate that the synthesized new iridium(III) complexes **9a–9c** can induce cell death *via* ROS-mediated mitochondrial dysfunction, apoptosis and ferroptosis.

Received 16th April 2025,
Accepted 18th May 2025

DOI: 10.1039/d5dt00899a

rsc.li/dalton

Introduction

According to relevant statistics, more than 10 million people die of cancer globally every year, making it the second leading cause of death worldwide.[1] The current main treatment for cancer includes surgery, radiotherapy, and chemotherapy, while anti-cancer drugs are the mainstay of tumor containment.[2] Cisplatin can exert anticancer activity by attacking multiple sites and inhibiting cell division, and it is widely used for treating various cancers.[3–5] However, cisplatin has serious adverse effects such as nephrotoxicity, immunity loss and ototoxicity, which pose a challenge to cancer treatment.[6] Photodynamic therapy (PDT) is an emerging and approved cancer treatment in clinical application. Unlike traditional treatments, PDT generates cytotoxic singlet oxygen through a chemical reaction, which leads to apoptosis by acting on cellular DNA and destroying mitochondrial function; it can also selectively act on cancer cells, which can improve therapeutic efficacy and reduce toxic side effects.[7–10]

In PDT, the design of a photosensitizer (PS) is critical to its therapeutic efficacy, and iridium complexes represent an efficient PS. Tong *et al.* synthesized four novel iridium compounds and found that the compounds exhibited significant photodynamic activity against cancer cells *in vitro* under irradiation.[11] Wang *et al.* found that the complex exhibits good biocompatibility, high oxygen generation capacity, and strong cytotoxicity against cancer cells.[12] In our previous work, we observed that the iridium(III) complex $[Ir(piq)_2(DBDIP)]PF_6$ (piq: 1-phenylisoquinoline; DBDIP: 2-(2,3-dihydrobenzo[*b*]-[1,4]dioxin-6-yl)-1*H*-imidazo[4,5-*f*][1,10]phenanthroline) shows no cytotoxic activity, with an IC_{50} > 100 μM. However, upon

[a]*School of Pharmacy, Guangdong Pharmaceutical University, Guangzhou, 510006, PR China. E-mail: lyjche@gdpu.edu.cn, wxzqq1234@gdpu.edu.cn*
[b]*School of Chemistry and Chemical Engineering, Guangdong Pharmaceutical University, Zhongshan, Guangdong, 528458, PR China. E-mail: xuli@gdpu.edu.cn*
† Electronic supplementary information (ESI) available. See DOI: https://doi.org/10.1039/d5dt00899a

irradiation, the complex exhibits a high inhibitory efficiency on cell proliferation in A549 cells.[13] We also found that [Ir(ppy)$_2$(MDIP)](PF$_6$) (ppy = 2-phenylpyridine, MDIP = 2-(7-methoxybenzo[*d*][1,3]dioxol-5-yl)-1*H*-imidazo[4,5-*f*][1,10]phenanthroline) can open mitochondrial permeability transition pore (MPTP) channel, cause a decrease in membrane potential, the release of cytochrome C, and activation of caspase 3, and finally lead to apoptosis upon irradiation conditions.[14] However, as one of the manners of cell death, ferroptosis has attracted great attention in recent years; several Ir(III) or Ru(II) complexes reduce glutathione (GSH), increase the amount of malondialdehyde (MDA), and downregulate the expression of GPX4, inducing ferroptosis.[15–18] To gain more insight and further understand possible anticancer mechanisms of iridium compounds as photosensitizers, herein, we synthesized a new ligand MHIP (2-(2-methyl-4-hydroxylphenyl)-1*H*-imidazo[4,5-*f*][1,10]phenanthroline) and three new iridium (III) complexes [Ir(ppy)$_2$(MHIP)](PF$_6$) (**9a**), [Ir(bzq)$_2$(MHIP)](PF$_6$) (**9b**), and [Ir(piq)$_2$(MHIP)](PF$_6$) (**9c**), (ppy = deprotonated 2-phenylpyridine, bzq = deprotonated benzo[*h*]quinoline, piq = deprotonated 1-phenylisoquinoline). The characterization of complexes was carried out by HRMS, ^{1}H NMR and ^{13}C NMR spectra; the anticancer activities and possible mechanism toward B16 cells were explored in detail.

Results and discussion

Chemistry

MHIP was synthesized by reacting 1,10-phenanthroline-5,6-dione with 4-hydroxy-2-methylbenzaldehyde. **9a–9c** were prepared by the reaction of MHIP with *cis*-[Ir(ppy)$_2$Cl]$_2$·H$_2$O, *cis*-[Ir(bzq)$_2$Cl]$_2$·H$_2$O or *cis*-[Ir(piq)$_2$Cl]$_2$·H$_2$O in dichloromethane and methanol (Scheme 1). The obtained complexes **9a–9c** were characterized by HRMS, ^{1}H and ^{13}C NMR spectra. In the HRMS spectra, the determined molecular weight of the complexes agreed with the calculated values. In the ^{1}H NMR spectra of MHIP, the peak of 2.62 ppm is assigned the –CH$_3$, and the peaks of 13.43 (s, 1H) and 9.81 (s, 1H) are attributed to the protons at the imidazole ring and –OH, while in the ^{1}H NMR spectra of the complexes, the peaks of 2.67 ppm for **9a**, 2.66 ppm for **9b** and 2.67 ppm for **9c** were attributed to the hydrogen atom on the methyl group. In addition, we did not observe the signal of the proton on the phenol hydroxyl group (–OH). Owing to a quick exchange between two nitrogen atoms in the imidazole ring, the signal of the proton in the imidazole ring was not observed. In the ^{13}C NMR spectra, the peaks of 21.64 ppm for MHIP, 21.74 ppm for **9a**, 21.93 ppm for **9b** and 21.91 ppm for **9c** are assigned to the carbon atom on the methyl group. The purity of **9a–9c** was determined by HPLC

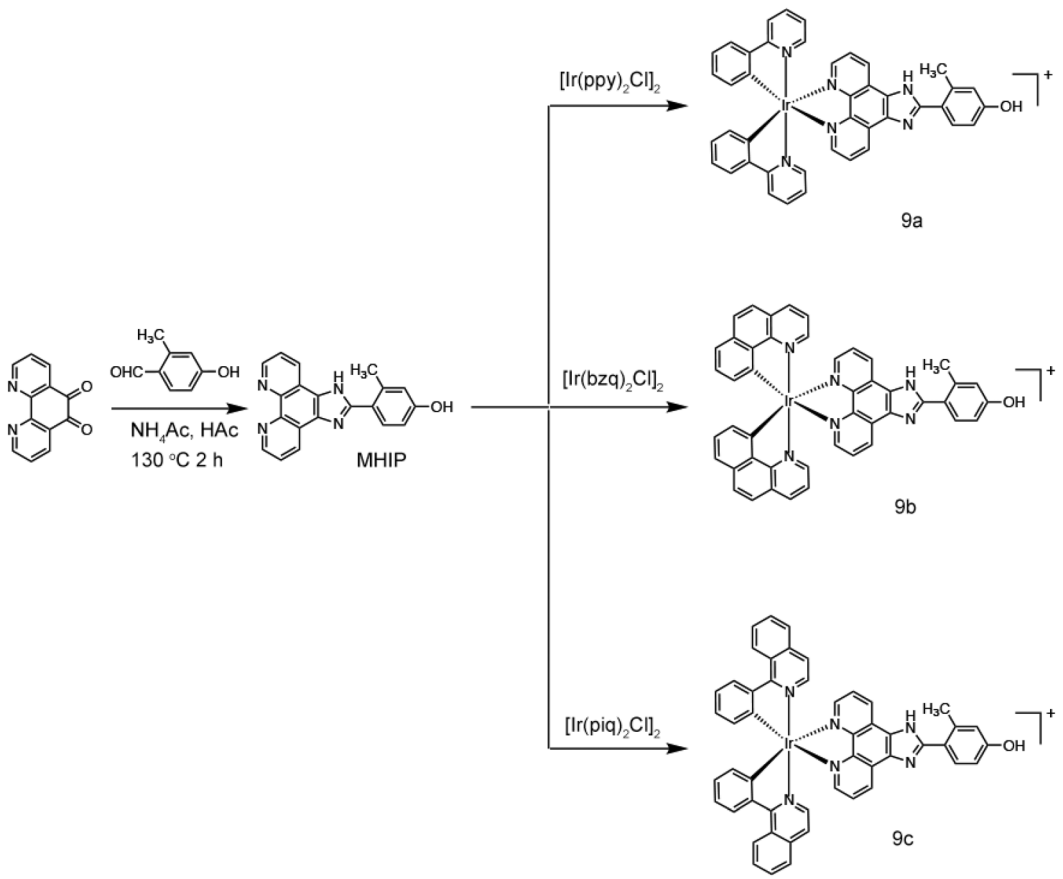

Scheme 1 Synthetic route to MHIP and **9a**, **9b** and **9c**.

(purity >95%) (Fig. S1, ESI†). Fig. S2a† shows UV-Vis spectra of complexes **9a–9c** in PBS, and the maximum absorbance appeared at 275 nm (ε = 37 450), 267 nm (ε = 29 000) and 290 nm (ε = 14 600). The complexes emit a weak fluorescence in PBS solution (Fig. S2b, ESI†), and the maximum peaks are located at 604 nm for **9a**, 600 nm for **9b** and 608 nm for **9c**. The stability of **9a**, **9b** and **9c** (10 μM) at 0, 24 and 48 h in PBS solution was determined, as shown in Fig. S2c (ESI†). No change in the peak shapes suggests that the complexes are stable in the PBS solution.

Cell uptake and cytotoxic activity *in vitro* studies

Before a compound can exert an anti-tumor effect, it first needs to enter cells. It is known that iridium(III) metal complexes can emit green fluorescence. To investigate whether iridium(III) complexes can enter the cells, B16 cells were exposed to twice IC_{50} concentrations of **9a**, **9b** and **9c** for 6 h. As illustrated in Fig. 1a, we discovered that **9a**, **9b** and **9c** can enter the cancer cells.

The antiproliferative activity of **9a**, **9b** and **9c** against HepG2, B16, A549 and normal NIH 3T3 was examined by 3-(4,5-dimethylthiazol-2-yl)-2,5-diphenyltetrazolium bromide (MTT).[19] The IC_{50} values are listed in Table 1. In the dark, it can be found that **9a**, **9b** and **9c** had moderate cytotoxicity on HepG2, A549 and B16 cells and no cytotoxicity toward NIH 3T3 cells. However, B16 cells were exposed to **9a–9c** for 4 h, irradiated for 30 min, and continuously cultured for 48 h. The three complexes showed enhanced cytotoxicity to both cancer and normal cells, among which the cytotoxicity to B16 cells was the largest, with IC_{50} values of 3.1 ± 0.3 μM, 4.9 ± 0.8 μM, and 0.4 ± 0.1 μM for **9a**, **9b** and **9c**, respectively; the cytotoxic activity of **9c** toward A549 cells is comparable to that of [Ir(bzq)$_2$(DBDIP)](PF$_6$) (IC_{50} = 0.4 μM).[13] Therefore, irradiation can significantly enhance the anticancer efficiency. In the subsequent cell experiments, except for cellular uptake and co-localization, B16 cells were treated with IC_{50} (or 2 × IC_{50}) of **9a**, **9b** and **9c** for 4 h, then irradiated for 30 min (white, LED lamp) and continuously cultured for 24 h.

Single oxygen and superoxide anions are all excited state molecules from the ROS family, which can easily bind to DNA, proteins, and other biomolecules, causing damage to the cell and finally leading to cell death.[20–24] 1,3-Diphenylisobenofuran (DPBF) is a fluorescent probe with high specificity for singlet oxygen. After binding to singlet oxygen, DPBF undergoes irreversible oxidation, thereby leading to a decrease in the intensity of ultraviolet absorption.[25] As depicted in Fig. 1b and c, the UV absorption value at 417 nm shows a decreasing trend, and changes in the absorbance of **9a**, **9b** and **9c** reach 79.1, 80.8 and 87.5%, respectively, which indicates that the complexes **9a–9c** produce singlet state oxygen during the light activation process. Additionally, we used Ru(bpy)$_3^{2+}$ as the standard (methanol, Φ = 0.81)[26] to determine the quantum yields based on the following equation:[27]

$$\Phi_{sample} = \Phi_{ref} \times (K_{sample}/K_{ref}) \times (F_{ref}/F_{sample}),$$

where K is the slope, F is the calibration factor of the absorbance, and $F = 1–10^{-OD}$ (OD is the absorbance of the photosensitizer at the light source wavelength). The quantum yields (Φ) were determined to be 0.56, 0.69 and 0.89 for **9a**, **9b** and **9c**, respectively. **9c** shows the highest quantum yield; hence, **9c** exhibits the highest cytotoxic activity among these complexes under irradiation conditions.

Dihydrorhodamine (DHR123) is a non-fluorescent active oxygen indicator that emits fluorescence when oxidized to a cationic state. We use it to indirectly measure the generation of superoxide anions.[28] As shown in Fig. 1d and e, the fluorescent intensity of DHR123 shows an increase of 3.42, 2.34 and 1.46 times for **9a**, **9b** and **9c**, respectively, compared to the control during 60 s irradiation time. The quantum yields were calculated using the following equation:

$$\Phi_S = \Phi_R \times (F_S/F_R) \times (A_R/A_S),$$

where S is the symbol of the samples, R is the symbol of the standard, Φ is the fluorescence quantum yield, F is the area under the fluorescence emission curves and A shows the absorbance at the excitation wavelength.

The quantum yields Φ were determined to be 0.0298, 0.0125 and 0.0671 for **9a**, **9b** and **9c**, respectively. These results suggest that **9a**, **9b** and **9c** can effectively produce singlet oxygen and superoxide anions.

Cell scratch, cloning and cell cycle arrest studies

Cancer is a global problem that threatens human health. Tumor cells can proliferate and invade indefinitely, which has created a great challenge for treatment.[29] To investigate the impact of **9a**, **9b** and **9c** on the proliferation and migration of B16 cells, we carried out cell cloning and scratch experiments. The results of the scratch experiments are shown in Fig. 2a and b. The cells treated with **9a–9c** show different degrees of migratory inhibition compared to the control. The cloning results are illustrated in Fig. 2c. Compared with the control group, the number of living cells in the complex-treated groups was greatly reduced, indicating that **9a**, **9b** and **9c** had a greater antiproliferative effect on B16 cell proliferation. FAK has a promotional effect on the growth and metastasis of tumor cells. Increased FAK expression has been shown in many primary and metastatic cancers.[30] Consequently, the change in FAK protein levels was investigated by western blot. Fig. 2d illustrates that the expression of FAK protein in the cells treated with **9a–9c** shows a downward trend in contrast to the control group, which further shows that the three complexes possess an inhibitory effect on the proliferation of B16 cells.

γ-H2AX is an important marker of DNA damage.[31,32] To investigate the extent of DNA damage in B16 cells induced by metal complexes **9a–9c**, we performed immunofluorescence staining of the cells using γ-H2AX dye. As shown in Fig. 2e, without the addition of the complex, the green fluorescence was very weak. However, after being treated with the complexes under irradiation conditions, the cells showed strong green fluorescence. It can be concluded that photoactivated metal

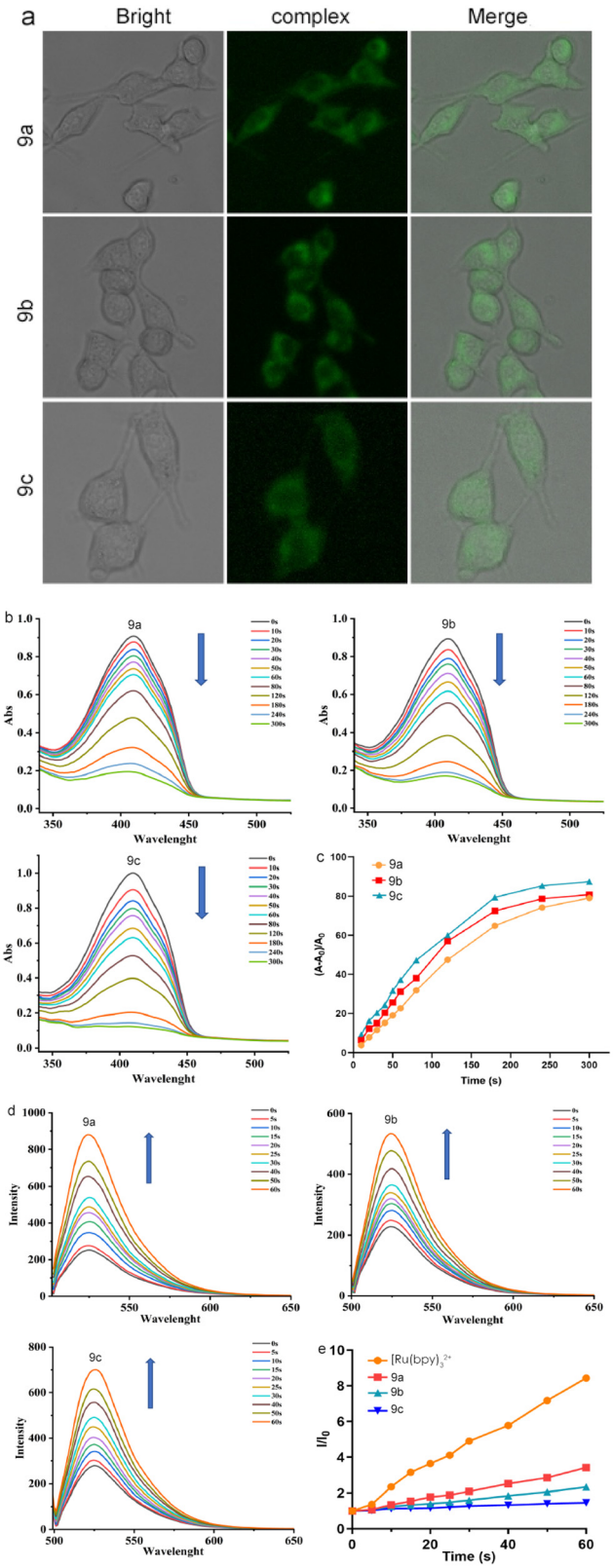

Fig. 1 (a) Cellular uptake, (b and c) single oxygen assay in the change in UV-Vis absorption spectra of DPBF (417 nm) after irradiation for 0–300 s. (d and e) Superoxide anion assay of the change in the fluorescent intensity of DHR123 (525 nm) during 0–60 s irradiation.

Table 1 IC_{50} values of compounds **9a–9c** for selected tumor cells and normal cells for 48 h

	B16		HepG2		A549		NIH 3T3	
Complex	$IC_{50\ dark}$	$IC_{50\ light}$	$IC_{50\ dark}$	$IC_{50\ light}$	$IC_{50\ dark}$	$IC_{50\ light}$	$IC_{50\ dark}$	$IC_{50\ light}$
9a	28.8 ± 1.3	3.1 ± 0.3	30.0 ± 4.0	9.3 ± 1.5	23.4 ± 1.2	15.9 ± 2.8	>100	>100
9b	26.1 ± 1.8	4.9 ± 0.8	19.2 ± 4.2	10.2 ± 3.1	23.8 ± 1.5	15.0 ± 2.0	>100	>100
9c	30.8 ± 3.1	0.4 ± 0.1	46.7 ± 2.4	4.5 ± 1.4	24.9 ± 0.4	0.5 ± 0.3	>100	21.7 ± 0.8
Cisplatin	9.1 ± 1.4		18.8 ± 1.2		6.6 ± 0.7		nd	

Data for cisplatin from ref. 18, nd: not determined.

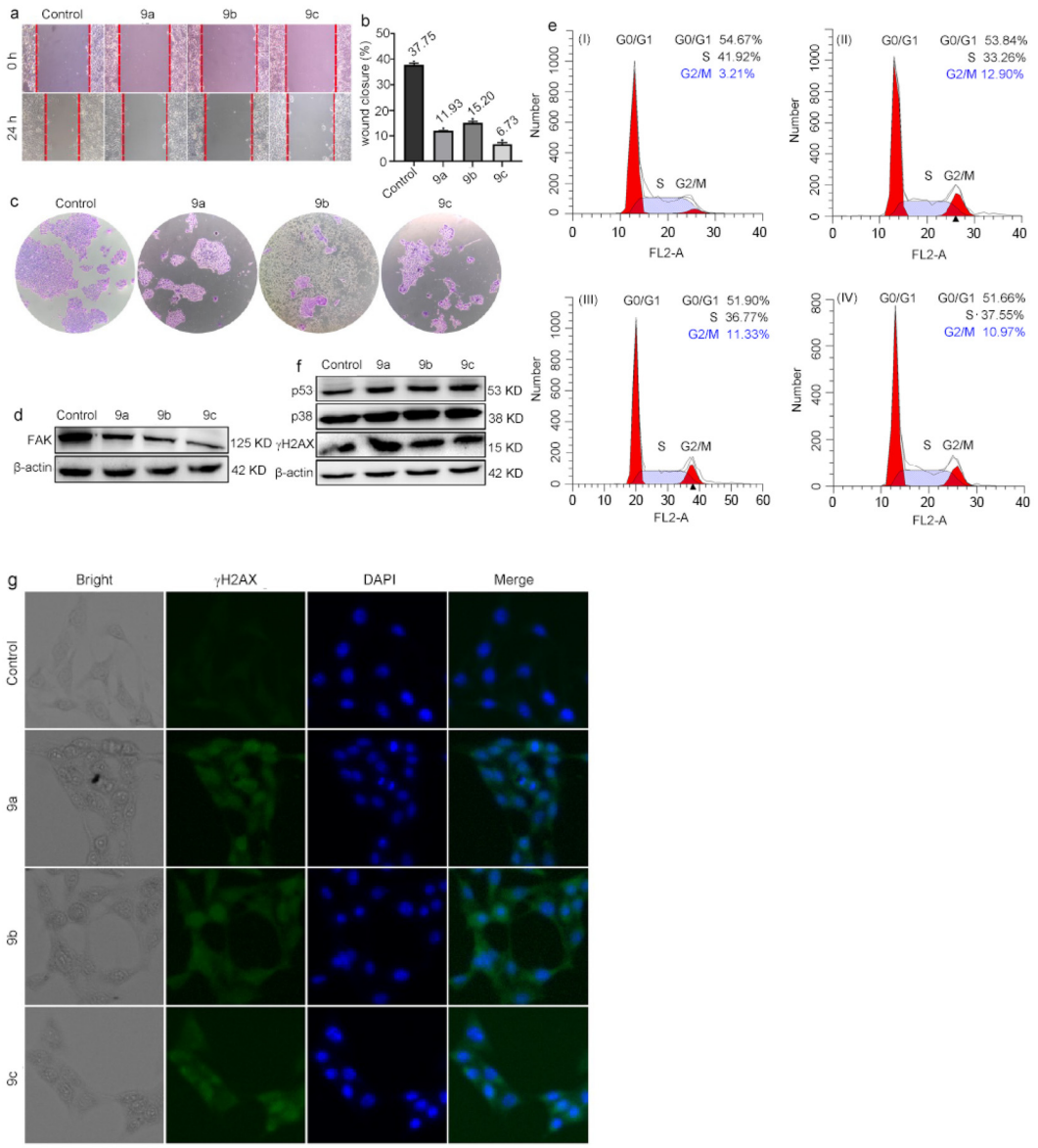

Fig. 2 (a and b) Wound healing assay; (c) cell colony; (d) expression of FAK; (e) cell cycle distribution, control (I), **9a** (II), **9b** (III) and **9c** (IV); (f) p53, p38 and γ-H2AX expression; (g) DNA damage assay was performed with B16 cells incubated with IC_{50} concentrations of **9a**, **9b** and **9c** for 4 h, then irradiated for 30 min, and continuously cultured for 24 h, while in the cell colony, after 30 min irradiation, the cells were continuously cultured for 7 days.

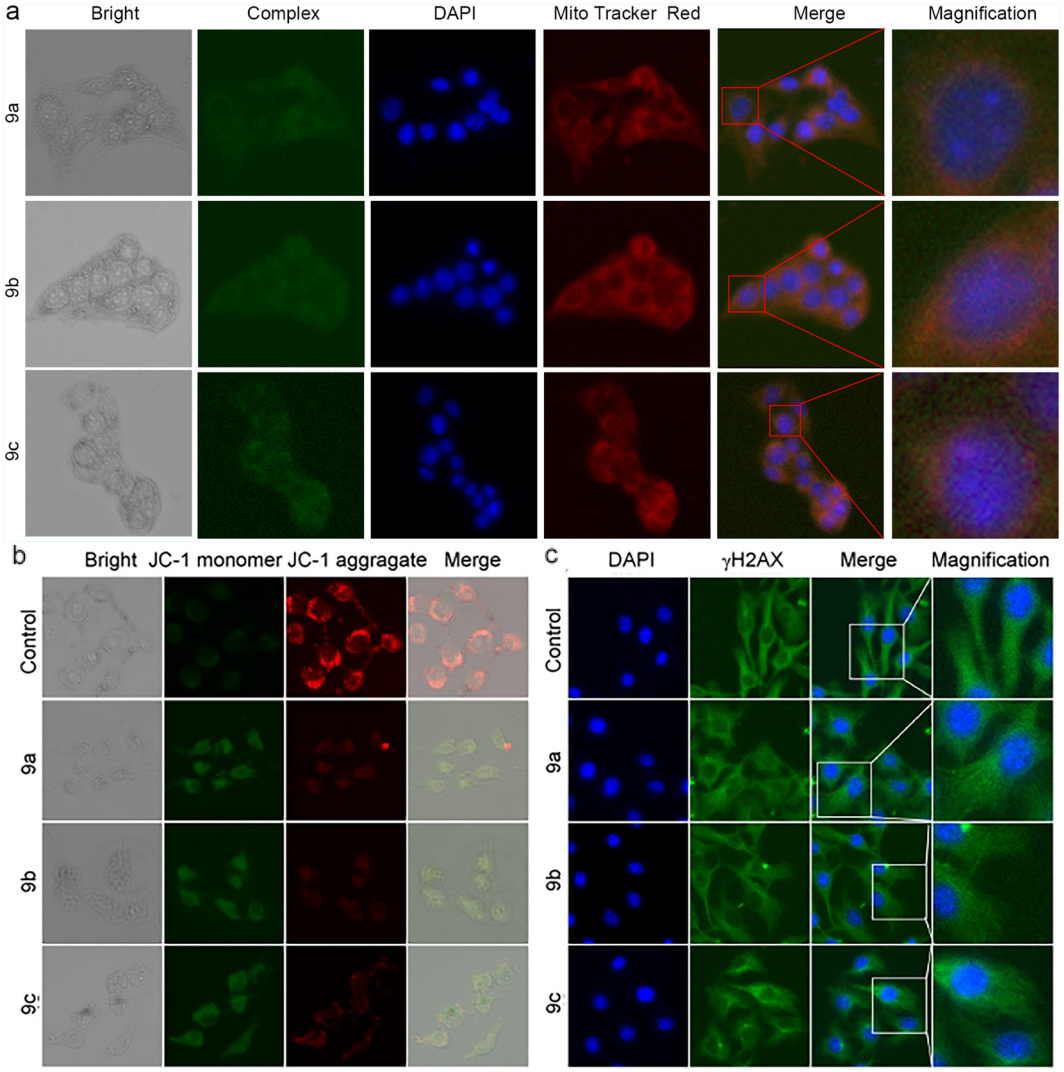

Fig. 3 (a) Co-localization of the complexes at the mitochondria, (b) assay of MMP, (c) assay of α-tubulin microtubule after B16 cells were treated with IC_{50} concentrations of **9a**, **9b** and **9c** for 4 h, irradiated for 30 min and continuously cultured for 24 h.

complexes **9a–9c** could induce cell death by causing DNA damage. In normal proliferating cells, a series of events, such as DNA replication and cell division, are in order.[33] The anticancer effect can be produced by interfering with the cell cycle of tumor cells.[34] We used flow cytometry to analyze the impact of **9a–9c** on the cell cycle distribution, and the results are shown in Fig. 2f. Compared to the control group, the percentage of the cells in the G1/G0 and S phases decreased after treatment with **9a**, **9b** and **9c**, and the percentage of the cells in the G2/M phase increased by about 9.69% for **9a**, 8.12% for **9b** and 7.76% for **9c**. These results suggest that **9a–9c** can inhibit cell proliferation in the G2/M phase. p53, p38 and γ-H2AX are closely related to the cell cycle. γ-H2AX is associated with DNA damage and can promote DNA repair.[35] The protein kinase p38 can activate protein p53,[36,37] which can regulate cell cycle progression.[38] Consequently, we examined the expression of p38, p53 and γ-H2AX. As shown in Fig. 2g, the expression of p53, p38 and γ-H2AX increased after the treatment of B16 cells with IC_{50} concentration of **9a–9c** upon irradiation. These results clearly demonstrate that **9a**, **9b** and **9c** can cause DNA damage and block cell proliferation at the G2/M phase.

Localization, membrane potential and microtubule morphology

Mitochondria can provide energy in eukaryotic cells, and they are also critical organelles that mediate the onset of apoptosis and senescence.[39] To investigate whether **9a–9c** can enter mitochondria, we performed a localization assay. Mito tracker red can stain mitochondria in living cells. As depicted in Fig. 3a, the cells were treated with IC_{50} concentrations of **9a**, **9b** and **9c** for 6 h, and the mitochondria were stained red. The overlap of red with green emitted by the complexes indicates that the complexes co-localize in the mitochondria.

Mitochondrial membrane potential (MMP) is an important indicator of cellular normalcy and is lost in the early stages of apoptosis.[40,41] JC-1 emits red fluorescence when the intracellular mitochondrial potential is sufficient, but the fluorescence changes to green when a decrease in MMP occurs.[42] The results of the MMP assay are presented in Fig. 3b. After treatment with the complexes, the red fluorescence was significantly weakened. However, green fluorescence was significantly enhanced compared to the control, indicating that **9a–9c** could trigger a decrease in MMP. Microtubules have a large impact on cellular functions, such as intracellular transport, cellular structure, and cell division.[43–46] Hence, we further tested the changes in microtubule morphology after treatment with the complexes. Fig. 3c depicts that the microtubule structure in the control was neatly and tightly arranged, whereas the structure began to become loose and unordered after treatment with **9a–9c**. The above results suggest that **9a**, **9b** and **9c** disrupt microtubule structure and thus trigger cell death.

Measurement of intracellular ROS generation and LDH release

Intracellular reactive oxygen species are highly active and produced within the mitochondria, which exert an influence on cellular metabolism by regulating signal transduction, inducing oxidative stress and causing DNA damage.[47] 2′,7′-Dichlorodihydro-fluorescein diacetate (DCHF-DA), as a non-fluorescent probe, is used to detect the level of intracellular ROS in cells.[48] In the presence of ROS, DCHF-DA is converted into characteristic green fluorescence 2′,7′-dichlorofluorescein (DCF). As illustrated in Fig. 4a, in the control, a weak green fluorescence was observed, while in the complex-treated groups, a bright green fluorescence was observed. Hence, the green fluorescence was significantly increased, suggesting that **9a**, **9b** and **9c** can elevate the intracellular ROS level. LDH is a cytoplasmic enzyme widely present in the cell, and when the cell is damaged or dies, LDH is released outside of the cell; therefore, we can validate the degree of cellular damage by quantitatively measuring the amount of released LDH.[49–51] Fig. 4b depicts that the cells treated with **9a–9c** showed an increase in the release of LDH compared to the control, indicating that the LDH was released outside of the cells. These results suggest that **9a**, **9b** and **9c** can promote B16 cell damage, which in turn induces cell death.

RNA sequencing

We constructed heat maps and volcano maps using R software to investigate whether **9c** can regulate gene expression. It can be observed from Fig. 5a and b that 1445 genes were regulated, among which 812 genes were upregulated and 633 genes were downregulated after B16 cells were treated with **9c** for 24 h. Meanwhile, to further explore the signaling pathways, GO analysis and KEGG pathway analysis were performed. As shown in Fig. 5c and d, GO analysis provided the number of proteins in the cellular component (CC, red) and biological process (BP, blue), which helps understand the function, localization, and biological pathways of proteins. KEGG enrichment clearly showed the metabolic pathways, which include the PI3K/AKT signaling pathway and glutathione metabolism. Overall, these results suggest that **9c** can cause a change in cellular gene expression and exert antitumor effects through relevant pathways.

Apoptosis and mechanism

Apoptosis allows organisms to maintain homeostatic levels by regulating the balance between cell proliferation and death.[52,53] However, unlimited proliferation of tumor cells and less apoptosis disrupts this balance.[54] To explore the apoptotic efficiency of **9a**, **9b** and **9c** on B16 cells, we used flow cytometry to examine the apoptotic percentage. Fig. 6a shows that the

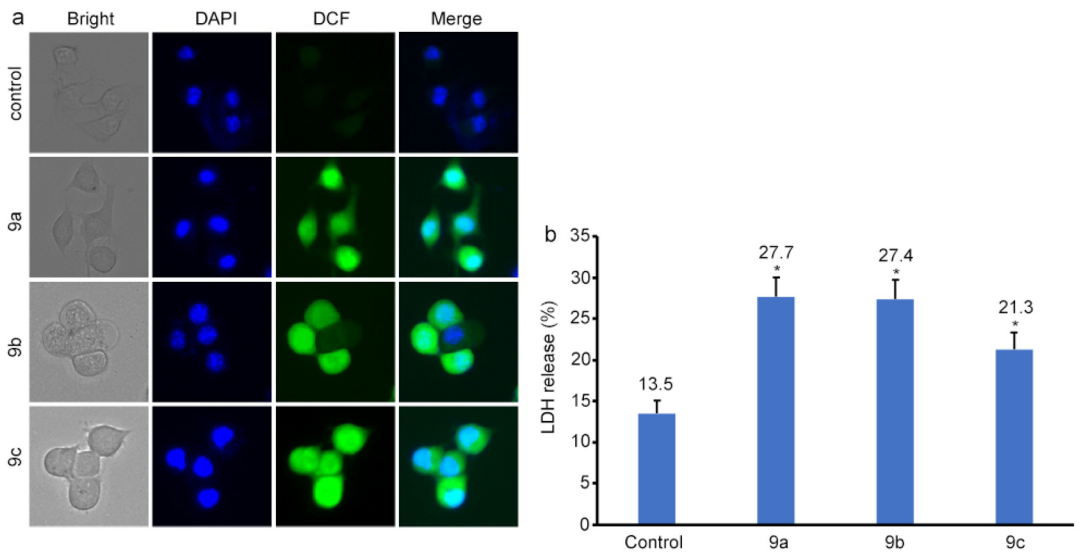

Fig. 4 (a) Intracellular ROS levels assay and (b) the release of LDH assay. B16 cells were cultured with IC_{50} concentrations of **9a–9c** for 4 h, irradiated for 30 min, and continuously cultured for 24 h.

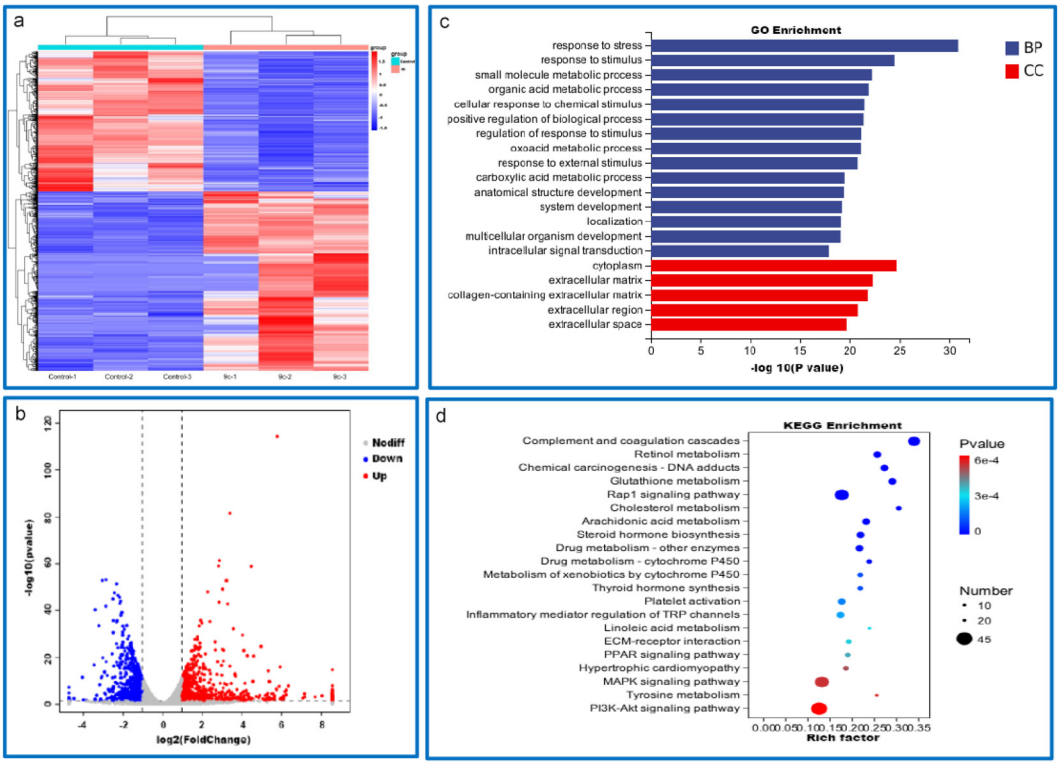

Fig. 5 Analysis of RNA sequencing after exposure of B16 to twice the IC_{50} concentration of **9c** for 4 h, irradiated for 30 min and continuously cultured for 24 h: (a) heat map, (b) volcano map, (c) GO analysis, and (d) KEGG enrichment analysis.

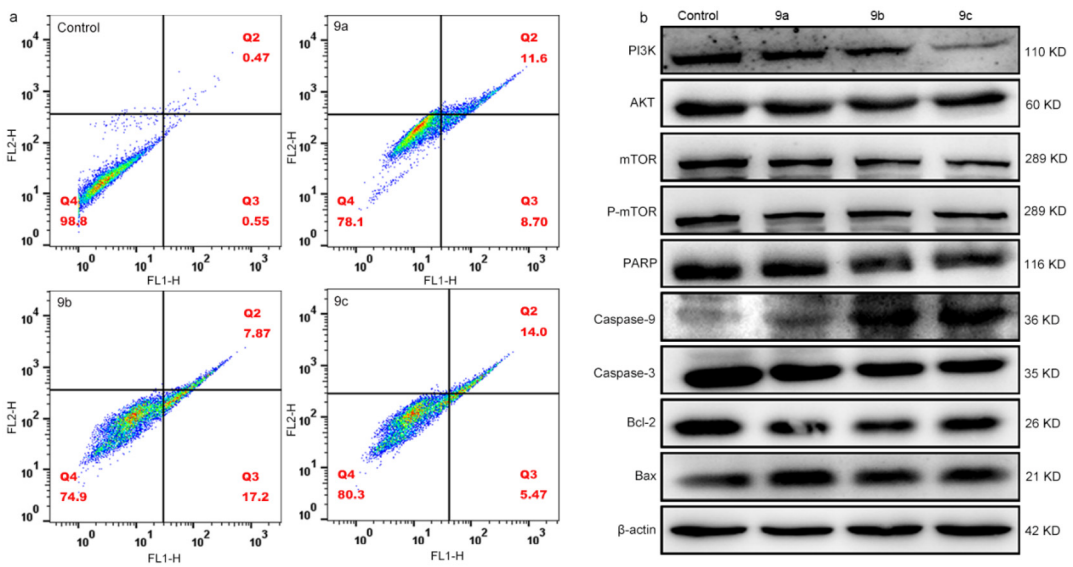

Fig. 6 (a) Effect of **9a–9c** on apoptosis. (b) The expression of relevant proteins in B16 cells. B16 cells were incubated with an IC_{50} concentration of **9a–9c** for 4 h, irradiated for 30 min and continuously cultured for 24 h.

percentage of early (Q2) and late (Q3) apoptotic cells increased to 19.28% for **9a**, 24.05% for **9b**, and 18.45% for **9c** compared to the control; meanwhile, the living cells (Q4) significantly decreased. These results suggest that **9a**, **9b** and **9c** can efficiently promote the apoptosis of B16 cells. Tumor progression can be inhibited by the inhibition of PI3K expression.[55–57] Therefore, we measured the expression of PI3K/AKT pathway-related proteins. It is well known that AKT activates Bax and inactivates Bcl-2 and caspase-9 proteins,[58–60] while mTOR is a major downstream target of the PI3K/AKT

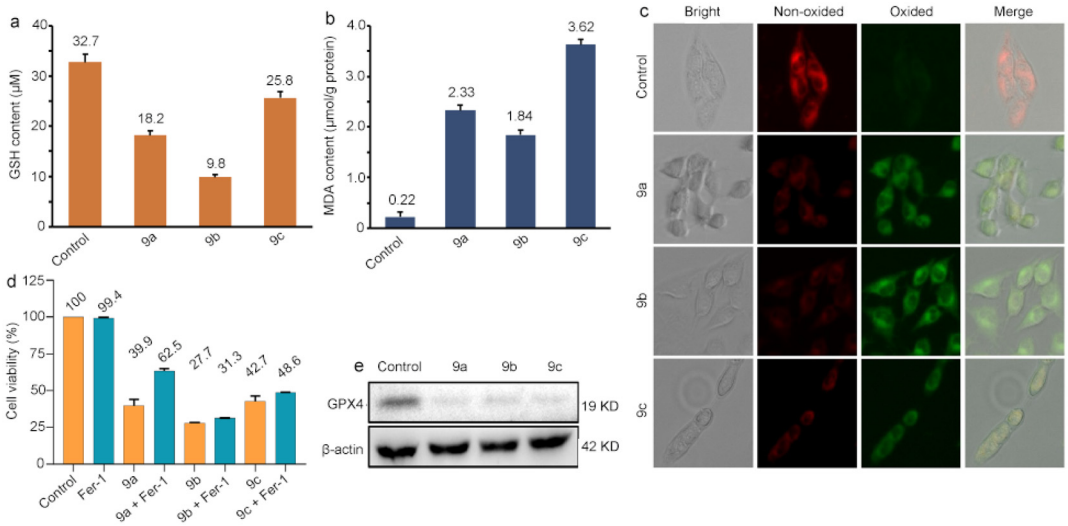

Fig. 7 (a) Intracellular GSH content, (b) intracellular MDA content, (c) lipid peroxidation assay using C11-BODIPY 581/591 as a fluorescence probe, (d) cell viability assay in the presence of Fer-1, and (e) expression level of intracellular GPX4 protein. B16 cells were exposed to IC_{50} concentrations of **9a**, **9b** and **9c** for 4 h, then irradiated for 30 min and continuously cultured for 24 h.

pathway, and a critical regulator of cellular metabolism.[61] As shown in Fig. 6b, the expression of PI3K, AKT, mTOR, and P-mTOR in B16 cells decreased compared to the control, which revealed that the PI3K/AKT signaling pathway was inhibited. In the caspase family, most proteins are associated with cell death or apoptosis,[62,63] and when caspase 9 is activated, it induces apoptosis by activating caspase 3, while caspase 3 can inhibit DNA repair.[64] Fig. 6b displays that the expression of Bax increased and that of Bcl-2 decreased, while the expression of caspase 9 increased and that of caspase 3 decreased in the caspase family. Meanwhile, we observed the downregulation of PARP. Therefore, we speculate that **9a**, **9b** and **9c** trigger apoptosis by ROS-mediated mitochondrial dysfunction and inhibit the PI3K/AKT signaling pathways.

Induction of ferroptosis

Ferroptosis is a mode of cell death regulated by oxidative and antioxidant systems, which produce lipid peroxides that lead to cell death.[65] Glutathione (GSH) plays a great role in maintaining intracellular redox homeostasis,[66] and the reduction of GSH levels triggers intracellular oxidative stress to induce ferroptosis.[67] First, we measured the effect of **9a–9c** on GSH content in B16 cells. The results can be observed in Fig. 7a. The contents of GSH in the cells treated with IC_{50} concentrations of **9a**, **9b** and **9c** were greatly reduced, which is caused by the reactive oxygen species to oxide GSH into glutathione disulfide (GSSG), inducing an imbalance of the redox system. MDA is a lipid peroxidation product and biomarker that can reflect the degree of lipid peroxidation.[68] Fig. 7b shows that a large increase in intracellular malondialdehyde (MDA) content was found compared to the control, indicating that lipid peroxidation occurred. Additionally, we applied C11-BODIPY 581/591 fluorescent probes to examine lipid peroxidation. By redox reaction with intracellular reactive oxygen species, the fluorescence changes from red to green, thus reflecting the intracellular lipid peroxidation level.[69,70] As shown in Fig. 7c, the significant reduction of red fluorescence and the enhancement of green fluorescence were observed after treatment of B16 cells with IC_{50} concentrations of **9a**, **9b** and **9c** for 24 h, indicating an incidence of lipid peroxidation. Ferrostatin-1 (Fer-1) is a selective inhibitor of ferroptosis, exerting its anti-ferroptotic activity by eliminating alkoxyl radicals in lipid hydroperoxides in the presence of ferrous ions.[71] Therefore, the Fer-1 inhibitor can be used to verify whether **9a**, **9b**, and **9c** can disrupt the lipid peroxidation balance in tumor cells. Therefore, we examined cell viability in the presence of Fer-1. As shown in Fig. 7d, Fer-1 promotes the increment of cell viability compared to the complex alone. GPX4 is a key regulator in the ferroptosis process,[72,73] and a decrease in its level makes cells more sensitive to ferroptosis. We used western blotting experiments to explore the expression of GPX4. Fig. 7e shows that the expression of GPX4 in the cells treated with **9a**, **9b** and **9c** demonstrated a decreasing trend. All these results indicate that **9a–9c** could reduce the content of GSH and downregulate the expression of GPX4, disrupt the balance of the intracellular redox system, promote the generation of cellular lipid peroxidation, and then induce the occurrence of ferroptosis.

Conclusions

In this study, three complexes, **9a–9c**, were successfully synthesized and characterized. In the MTT experiments, we found that the three complexes exhibited significant cytotoxicity to B16 cells after irradiation. Cellular uptake and co-localization assays found that the complexes can enter the cells and localize in the mitochondria. Increased expression of p38 and γ-H2AX indicated that DNA damage occurred in the B16 cells.

Reduced glutathione (GSH) concentration, increased malondialdehyde (MDA) levels, down-regulation of GPX4 expression, and C11-BODIPY581/591 staining results demonstrate that the complexes induce ferroptosis. In conclusion, the present study demonstrates that newly synthesized iridium(III) complexes can induce cell death *via* apoptosis (a ROS-mediated mitochondrial dysfunction pathway) and ferroptosis. This work provides some insights into the anticancer activity of iridium(III) complexes and helps in the design and synthesis of new iridium (III) complexes as drug candidates.

Experimental

Synthesis of ligands and complexes

Synthesis of ligand MHIP. A mixture of phenanthroline-5,6-dione (0.315 g, 1.5 mmol), 2-methyl-4-hydroxyl-benzaldehyde (0.189 g, 1.5 mmol), and NH_4Ac (2.31 g, 30 mmol) was completely dissolved in 25 mL of acetic acid and refluxed at 130 °C for 2 h. After the solution was cooled, the solution was neutralized with concentrated $NH_3{\cdot}H_2O$, the yellow precipitate was washed with ice water, and the yellow powder was obtained. Yield: 80% (0.391 g). HRMS (CH_3OH): m/z = 325.0999 $[M - H]^-$. ^1H NMR (DMSO-d_6, 500 MHz): 13.34 (s, 1H), 9.81 (s, 1H), 8.98 (d, 2H, J = 4.5 Hz), 8.86 (d, 2H, J = 8.0 Hz), 7.81–7.76 (m, 2H), 7.66 (d, 1H, J = 8.5 Hz), 6.79 (d, 2H, J = 8.5 Hz), 2.62 (s, 3H). ^{13}C NMR (DMSO-d_6, 125 MHz): 158.74, 152.14, 148.06, 147.99, 143.93, 143.73, 139.28, 135.86, 131.41, 129.99, 125.90, 124.35, 123.82, 123.55, 121.40, 119.80, 118.39, 113.43, 21.64.

Synthesis of complexes

The mixture of MHIP (0.326 g, 1 mmol) and *cis*-$[Ir(ppy)_2Cl]_2{\cdot}H_2O$[74] (0.56 g, 0.5 mmol) or *cis*-$[Ir(bzq)_2Cl]_2{\cdot}H_2O$[74] or *cis*-$[Ir(piq)_2Cl]_2{\cdot}H_2O$[74] was weighed precisely and placed in a three-necked flask. CH_2Cl_2 (20 mL) and CH_3OH (10 mL) were added as solvents. The reaction was carried out at 40 °C under argon. After 6 h, the reaction was added to an appropriate amount of NH_4PF_6 powder (about 1 g) to continue for 1 h. The yellow crude product was obtained after filtration. Then, the crude product was purified by column chromatography using dichloromethane and acetone as eluents.

9a: yield, 82%. ^1H NMR (DMSO-d_6, 500 MHz, Fig. S3, ESI†): 9.28 (d, J = 6.0 Hz, 2H), 8.26 (d, J = 8.0 Hz, 2H), 8.11 (d, J = 6.0 Hz, 2H), 8.04 (dd, J = 8.0 Hz, 2H), 7.95 (d, J = 7.5 Hz, 2H), 7.88 (t, J = 7.5 Hz, 2H), 7.80 (d, J = 8.5 Hz, 1H), 7.51 (d, J = 5.5 Hz, 2H), 7.06 (t, J = 7.5 Hz, 2H), 6.99–6.93 (m, 4H), 6.83 (d, J = 9.0 Hz, 2H), 6.30 (d, J = 7.5 Hz, 2H), 2.67 (s, 3H). ^{13}C NMR (DMSO-d_6, 125 MHz, Fig. S4, ESI†): 167.35, 159.14, 151.04, 149.61, 148.36, 144.52, 144.23, 139.47, 139.10, 132.83, 131.84, 131.71, 130.70, 127.26, 125.52, 124.30, 122.78, 121.10, 120.41, 118.46, 113.56, 21.74. HRMS (CH_3CN): calcd for $C_{42}H_{30}IrN_6OPF_6$: m/z = 827.2110 $([M - PF_6])^+$, found: m/z = 827.2106 $([M - PF_6])^+$.

9b: yield, 74%. ^1H NMR (DMSO-d_6, 500 MHz, Fig. S5, ESI†): 9.26 (d, J = 8.0 Hz, 2H), 8.51 (d, J = 7.5 Hz, 2H), 8.08 (d, J = 6.0 Hz, 2H), 7.98 (d, J = 8.5 Hz, 4H), 7.94–7.87 (m, 4H), 7.82 (d, J = 8.5 Hz, 1H), 7.57 (d, J = 8.0 Hz, 2H), 7.44 (dd, J = 8.0 Hz, 2H), 7.22 (t, J = 7.5 Hz, 2H), 6.82 (d, J = 9.0 Hz, 2H), 6.33 (d, J = 7 Hz, 2H), 2.66 (s, 3H). ^{13}C NMR (DMSO-d_6, 125 MHz, Fig. S6, ESI†): 159.03, 156.91, 149.31, 148.68, 147.91, 144.57, 140.87, 139.38, 137.96, 134.21, 132.83, 131.85, 130.18, 129.94, 129.04, 127.15, 124.69, 123.23, 120.76, 118.43, 113.52, 21.93. HRMS (CH_3CN): calcd for $C_{46}H_{30}IrN_6OPF_6$: m/z = 875.2110 $([M - PF_6])^+$, found: m/z = 875.2105 $([M - PF_6])^+$.

9c: yield, 80%, ^1H NMR (DMSO-d_6, 500 MHz, Fig. S7, ESI†): 9.31 (d, J = 7.5 Hz, 2H), 9.01 (d, J = 7.5 Hz, 2H), 8.40 (d, J = 8.0 Hz, 2H), 8.03–7.94 (m, 6H), 7.89–7.85 (m, 5H), 7.43 (d, J = 6.5 Hz, 2H), 7.38 (d, J = 6.5 Hz, 2H), 7.16 (t, J = 8.5 Hz, 2H), 6.96 (t, J = 7.5 Hz, 2H), 6.81 (d, J = 9.0 Hz, 2H), 6.30 (d, J = 7.0 Hz, 2H), 2.67 (s, 3H). ^{13}C NMR (DMSO-d_6, 125 MHz, Fig. S8, ESI†): 168.31, 158.94, 154.57, 148.00, 145.85, 143.92, 141.22, 139.33, 136.94, 132.91, 132.46, 132.17, 131.90, 130.98, 129.81, 128.15, 127.09, 126.89, 126.00, 122.65, 118.40, 113.49, 21.91. HRMS (CH_3CN): calcd for $C_{50}H_{34}IrN_6OPF_6$: m/z = 927.2423 $([M - PF_6])^+$, found: m/z = 927.2476 $([M - PF_6])^+$.

Single oxygen and superoxide anion detection

Single oxygen ($^1O_2$) is an essential substance in the process of killing tumor cells by photosensitizers. Similar to superoxide anions ($O_2^{\bullet-}$), they both belong to the ROS family and can directly or indirectly react with biological macromolecules to cause oxidative stress and damage, eventually triggering cell death. To investigate whether **9a**, **9b** and **9c** produce single oxygen and superoxide anion in the treatment process, we conducted these experiments using 1,3-diphenylisobenofuran (DPBF) and dihydrorhodamine (DHR123) as quenching agents. The UV-Vis spectra of the mixed solution containing 10 μM of DPBF and 10 μM of complexes in methanol solution were recorded after irradiation at 0 s, 10 s, 20 s, 30 s, 40 s, 50 s, 60 s, 80 s, 120 s, 180 s, 240 s, and 300 s. To determine $O_2^{\bullet-}$, we recorded the fluorescence spectra of the mixed solution of DHR123 (1 mM) with complexes in PBS after 0 s, 5 s, 10 s, 15 s, 20 s, 25 s, 30 s, 40 s, 50 s, and 60 s of illumination.

Cell apoptosis by flow cytometry

After the cells grew to a fusion degree of 80%–90% in 6-well plates, the cells were treated with 3.1 μM **9a**, 4.9 μM **9b** and 0.4 μM **9c** for 4 h and irradiated for 30 min. The cells were continuously cultured for 24 h. Then, the cells were digested and washed twice with PBS. Finally, the cells were stained with 195 μL of Annexin-FITC conjugate, 10 μL of PI staining solution, and 5 μL of Annexin V in the dark, and the apoptotic percentage of the cells was examined with flow cytometry.

Western blotting assay

When the cells grew to 80% in six-well plates, the cells were exposed to IC_{50} concentrations of **9a**, **9b** and **9c** for 4 h and irradiated for 30 min. Then, the cells were continuously cultured for 24 h. The total protein was extracted and determined by applying the BCA method. The protein was diluted to the same concentration with a protein loading detection buffer and deionized water, and the protein was boiled for 10 min to facilitate the preservation of the sample. Subsequently, the

various proteins were separated by sodium dodecyl sulfate-polyacrylamide gel electrophoresis (SDS-PAGE), and the proteins were transferred to a polyvinylidene fluoride (PVDF) membrane. The membranes were incubated overnight in primary antibody diluent, washed, and then incubated in secondary antibody diluent for 70 min. Protein bands were dyed in a chemiluminescence kit, and the results were analyzed as soon as possible using a FluorChem E instrument.

RNA sequencing assay

B16 cells were treated with **9c** ($2 \times IC_{50}$ concentration) for 4 h in six-well plates and illuminated for 30 min. The cells were continuously cultured for 24 h. The total RNA was extracted by adding Trizol reagent and quantitatively determined by applying a NanoDrop spectrophotometer.[75] Measurements were completed and quantified using the AMpure XP system (Beckman Coulter, Beverly, CA, USA), a 2100 system (Agilent, Santa Clara, CA, USA), and finally sequenced using the Illumina NextSeq 500 sequencing platform.

Note: The Materials and methods and the subsequent Experimental procedures can be found in the ESI.†

Cell culture, cytotoxicity assay, cellular uptake, cell colony assay and wound healing assay, cell cycle arrest analysis, mitochondrial localization and membrane potential measurement, cell microtubule morphology assay, DNA damage detection by γ-H2AX, determination of GSH and MDA content, C11-BODIPY 581/591 detection of ferroptosis, LDH release, intracellular ROS generation, and ferroptosis inhibitor.

Data analysis

Statistical significance was assessed with *t*-tests, and $*P < 0.05$ is significant.

Data availability

Data will be made available upon request.

Conflicts of interest

The authors declare no competing interest.

Acknowledgements

We are grateful for the National Natural Science Foundation of China (no. 21877018) and Discipline Training Excellence, Innovation and Quality Improvement Engineering Team Project (no. 2024ZZ05).

References

1 F. J. Sulzmaier, C. Jean and D. D. Schlaepfer, FAK in cancer: mechanistic findings and clinical applications, *Nat. Rev. Cancer*, 2014, **14**, 598–610.
2 E. Pérez-Herrero and A. Fernández-Medarde, Advanced targeted therapies in cancer: Drug nanocarriers, the future of chemotherapy, *Eur. J. Pharm. Biopharm.*, 2015, **93**, 52–79.
3 S. Ghosh, Cisplatin: The first metal based anticancer drug, *Bioorg. Chem.*, 2019, **88**, 102925.
4 A. M. P. Romani, Cisplatin in cancer treatment, *Biochem. Pharmacol.*, 2022, **206**, 115323.
5 X. Wang, Y. Zhou, D. Wang, Y. Wang, Z. Zhou, X. Ma, X. Liu and Y. Dong, Cisplatin-induced cytotoxicity: From signaling network to therapeutic targets, *Biomed. Pharmacother.*, 2023, **157**, 114045.
6 S. Dasari and P. B. Tchounwou, Cisplatin in cancer therapy: molecular mechanisms of action, *Eur. J. Pharmacol.*, 2014, **740**, 364–378.
7 B. Ji, M. Wei and B. Yang, Recent advances in nanomedicines for photodynamic therapy (PDT)-driven cancer immunotherapy, *Theranostics*, 2022, **12**, 434–458.
8 P. Agostinis, K. Berg, K. A. Cengel, T. H. Foster, A. W. Girotti, S. O. Gollnick, S. M. Hahn, M. R. Hamblin, A. Juzeniene, D. Kessel, M. Korbelik, J. Moan, P. Mroz, D. Nowis, J. Piette, B. C. Wilson and J. Golab, Photodynamic therapy of cancer: an update, *CA-Cancer J. Clin.*, 2011, **61**, 250–281.
9 D. E. Dolmans, D. Fukumura and R. K. Jain, Photodynamic therapy for cancer, *Nat. Rev. Cancer*, 2003, **3**, 380–387.
10 B. M. Luby, C. D. Walsh and G. Zheng, Advanced photosensitizer activation strategies for smarter photodynamic therapy beacons, *Angew. Chem., Int. Ed.*, 2019, **58**, 2558–2569.
11 J. Tong, X. Yang, X. Song, J. Liang, S. Huang, H. Mao, M. Akhtar, A. Liu, G. G. Shan and G. Li, AIE-active Ir(III) complexes as type-I dominant photosensitizers for efficient photodynamic therapy, *Dalton Trans.*, 2023, **52**, 1105–1112.
12 Z. Wang, L. Li, W. Wang, R. Wang, G. Li, H. Bian, D. Zhu and M. R. Bryce, Self-assembled nanoparticles based on cationic mono-/AIE tetra-nuclear Ir(III) complexes: long wavelength absorption/near-infrared emission photosensitizers for photodynamic therapy, *Dalton Trans.*, 2023, **52**, 1595–1601.
13 L. Zhou, J. B. Li, J. Chen, X. Yao, X. D. Zeng, Y. J. Liu, Y. Wang and X. Z. Wang, Anticancer activity and mechanism studies of photoactivated iridium(III) complexes toward lung cancer A549, *Dalton Trans.*, 2024, **53**, 15176–15189.
14 G. C. Li, J. Chen, Y. F. Xie, Y. Yang, Y. J. Niu, X. L. Chen, L. Zhou and Y. J. Liu, White light. increases anticancer effectiveness of iridium(III) complexes toward lung cancer A549 cells, *J. Inorg. Biochem.*, 2024, **259**, 112652.
15 S. Tian, H. X. Xu, X. Y. Wu, Y. Y. Ding, L. J. Liang, H. Yin, X. D. Zeng, Y. J. Liu and W. R. Zhu, Ruthenium(II) polypyridyl complexes inhibit tumor growth through stimulating immune system to increase $CD8^+$ T Cell, *Eur. J. Med. Chem.*, 2025, **290**, 117470.
16 H. Y. Hu, J. Chen, F. Zhang, Z. J. Sheng, Y. Yang, Y. F. Xie, L. Zhou and Y. J. Liu, Evaluation of efficiency of liposome-entrapped Iridium(III) complexes Inhibiting tumor growth in vitro and in vivo, *J. Med. Chem.*, 2024, **67**, 16195–16208.

17 H. W. Zhang, K. Wang, D. L. Ji, X. Liu, C. Wang, Y. Y. Jiang, Z. H. Jia, B. Xiong, Y. Ling and J. F. Miao, Novel tris-bipyridine based Ru(II) complexes as type-I/-II photosensitizers for antitumor photodynamic therapy through ferroptosis and immunogenic cell death, *Eur. J. Med. Chem.*, 2024, **279**, 116909.
18 C. X. Huang, Y. H. Yuan, G. C. Li, S. Tian, H. Y. Hu, J. Chen, L. J. Liang, Y. Wang and Y. J. Liu, Mitochondria-targeted iridium(III) complexes encapsulated in liposome induce cell death through ferroptosis and gasdermin-mediated pyroptosis, *Eur. J. Med. Chem.*, 2024, **266**, 116112.
19 T. Mosmann, Rapid colorimetric assay for cellular growth and survival: application to proliferation and cytotoxicity assays, *J. Immunol. Methods*, 1983, **65**, 55–63.
20 X. Zheng and Q. Huang, Assessment of the antioxidant activities of representative optical and geometric isomers of astaxanthin against singlet oxygen in solution by a spectroscopic approach, *Food Chem.*, 2022, **395**, 133584.
21 A. Krieger-Liszkay, Singlet oxygen production in photosynthesis, *J. Exp. Bot.*, 2005, **56**, 337–346.
22 P. Di Mascio, G. R. Martinez, S. Miyamoto, G. E. Ronsein, M. H. G. Medeiros and J. Cadet, Singlet molecular oxygen reactions with nucleic acids, lipids, and proteins, *Chem. Rev.*, 2019, **119**, 2043–2086.
23 W. Liu, S. He, X. Ma, C. Lv, H. Gu, J. Cao, J. Du, W. Sun, J. Fan and X. Peng, Near-infrared heptamethine cyanine photosensitizers with efficient singlet oxygen generation for anticancer photodynamic therapy, *Angew. Chem., Int. Ed.*, 2024, **63**, e202411802.
24 J. Zhang, Y. Wei, Y. Yue, H. Jiao, Y. Wu, W. Fu, K. M. Lin, C. Lu, S. Mou and Q. Zhong, IPK4 promotes oxidative stress and ferroptotic death through the downregulation of ACSM1, *Proc. Natl. Acad. Sci. U. S. A.*, 2024, **121**, e2410628121.
25 X. Ouyang, X. Wang, H. B. Kraatz, S. Ahmadi, J. Gao, Y. Lv, X. Sun and Y. Huang, A Trojan horse biomimetic delivery strategy using mesenchymal stem cells for PDT/PTT therapy against lung melanoma metastasis, *Biomater. Sci.*, 2020, **8**, 1160–1170.
26 K. Bhattacharyya and P. K. Das, Quantitative aspects of all-trans-retinol singlet and. triplet quenching by oxygen, *Chem. Phys. Lett.*, 1985, **116**, 326–331.
27 L. V. Lutkus, S. S. Rickenbach and T. M. Mccormick, Singlet oxygen quantum yields determined by oxygen consumption, *J. Photochem. Photobiol., A*, 2019, **378**, 131–135.
28 Z. Wang, L. Wei, J. Lin, C. Huang, H. Chen, D. Fan, W. Hu, J. Liu, H. Huang, Z. Wang and X. Wang, Donor-acceptor-donor strategy rouses the photodynamic therapy anticancer activity of a bis-terpyridyl Ru(II) complex, *J. Med. Chem.*, 2024, **67**, 13435–13445.
29 M. A. Zaimy, N. Saffarzadeh, A. Mohammadi, H. Pourghadamyari, P. Izadi, A. Sarli, L. K. Moghaddam, S. R. Paschepari, H. Azizi, S. Torkamandi and J. Tavakkoly-Bazzaz, New methods in the diagnosis of cancer and gene therapy of cancer based on nanoparticles, *Cancer Gene Ther.*, 2017, **24**, 233–243.
30 B. Y. Lee, P. Timpson, L. G. Horvath and R. J. Daly, FAK signaling in human cancer as a target for therapeutics, *Pharmacol. Ther.*, 2015, **146**, 132–149.
31 Q. Liu, Z. Lei, C. Gu, J. Guo, H. Yu, Z. Fatima, K. Zhou, M. A. B. Shabbir, M. K. Maan, Q. Wu, S. Xie, X. Wang and Z. Yuan, Mequindox induces apoptosis, DNA damage, and carcinogenicity in Wistar rats, *Food Chem. Toxicol.*, 2019, **127**, 270–279.
32 K. Khan, S. Tewari, N. P. Awasthi, S. P. Mishra, G. R. Agarwal, M. Rastogi and N. Husain, Flow cytometric detection of gamma-H2AX to evaluate DNA damage by low dose diagnostic irradiation, *Med. Hypotheses*, 2018, **115**, 22–28.
33 L. Dewachter, N. Verstraeten, M. Fauvart and J. Michiels, An integrative view of cell cycle control in Escherichia coli, *FEMS Microbiol. Rev.*, 2018, **42**, 116–136.
34 J. Li and B. Z. Stanger, Cell cycle regulation meets tumor immunosuppression, *Trends Immunol.*, 2020, **41**, 859–863.
35 S. Riffle, R. N. Pandey, M. Albert and R. S. Hegde, Linking hypoxia, DNA damage and proliferation in multicellular tumor spheroids, *BMC Cancer*, 2017, **17**, 338.
36 X. Wang, E. R. Simpson and K. A. Brown, p53: Protection against tumor growth beyond effects on cell cycle and apoptosis, *Cancer Res.*, 2015, **75**, 5001–5007.
37 T. M. Thornton and M. Rincon, Non-classical p38 map kinase functions: cell cycle checkpoints and survival, *Int. J. Biol. Sci.*, 2009, **5**, 44–51.
38 R. H. Whitaker and J. G. Cook, Stress Relief Techniques: p38 MAPK Determines the Balance of Cell Cycle and Apoptosis Pathways, *Biomolecules*, 2021, **11**, 1444.
39 S. C. H. Rehfeldt, S. Laufer and M. I. Goettert, A highly selective in vitro JNK3 inhibitor, FMU200, restores mitochondrial membrane potential and reduces oxidative stress and apoptosis in SH-SY5Y cells, *Int. J. Mol. Sci.*, 2021, **22**, 3701.
40 A. Cossarizza, C. Franceschi, D. Monti, S. Salvioli, E. Bellesia, R. Rivabene, L. Biondo, G. Rainaldi, A. Tinari and W. Malorni, Protective effect of N-acetylcysteine in tumor necrosis factor-alpha-induced apoptosis in U937 cells: the role of mitochondria, *Exp. Cell Res.*, 1995, **220**, 232–240.
41 A. Perelman, C. Wachtel, M. Cohen, S. Haupt, H. Shapiro and A. Tzur, JC-1: alternative excitation wavelengths facilitate mitochondrial membrane potential cytometry, *Cell Death Dis.*, 2012, **3**, e430.
42 K. Elefantova, B. Lakatos, J. Kubickova, Z. Sulova and A. Breier, Detection of the mitochondrial membrane potential by the cationic dye JC-1 in L1210 cells with massive overexpression of the plasma membrane ABCB1 drug transporter, *Int. J. Mol. Sci.*, 2018, **19**, 1985.
43 P. Binarová and J. Tuszynski, Tubulin: structure, functions and roles in disease, *Cells*, 2019, **8**, 1294.
44 E. D. McKenna, S. L. Sarbanes, S. W. Cummings and A. Roll-Mecak, The tubulin code, from molecules to health

and disease, *Annu. Rev. Cell Dev. Biol.*, 2023, **39**, 331–361.
45 M. O. Altonsy, A. Ganguly, M. Amrein, P. Surmanowicz, S. S. Li, G. J. Lauzon and P. R. Mydlarski, Beta3-tubulin is critical for microtubule dynamics, cell cycle regulation, and spontaneous release of microvesicles in human malignant melanoma cells (A375), *Int. J. Mol. Sci.*, 2020, **21**, 1656.
46 T. T. Miao, X. B. Tao, D. D. Li, H. Chen, X. Y. Jin, Y. Geng, S. F. Wang and W. Gu, Synthesis and biological evaluation of 2-aryl-benzimidazole derivatives of dehydroabietic acid as novel tubulin polymerization inhibitors, *RSC Adv.*, 2018, **8**, 17511–17526.
47 Z. Zou, H. Chang, H. Li and S. Wang, Induction of reactive oxygen species: an emerging approach for cancer therapy, *Apoptosis*, 2017, **22**, 1321–1335.
48 W. Xie, M. Peng, Y. Liu, B. Zhang, L. Yi and Y. Long, Simvastatin induces pyroptosis via ROS/caspase-1/GSDMD pathway in colon cancer, *Cell Commun. Signaling*, 2023, **21**, 329.
49 N. Abutaha, Apoptotic potential and chemical composition of Jordanian propolis extract against different cancer cell lines, *J. Microbiol. Biotechnol.*, 2019, **30**, 893–902.
50 C. Durchschein, A. Hufner, B. Rinner, A. Stallinger, A. Deutsch, B. Lohberger, R. Bauer and N. Kretschmer, Synthesis of novel shikonin derivatives and pharmacological effects of cyclopropylacetylshikonin on melanoma Cells, *Molecules*, 2018, **23**, 2820.
51 J. Li, S. H. Deng, J. Li, L. Li, F. Zhang, Y. Zou, D. M. Wu and Y. Xu, Obacunone alleviates ferroptosis during lipopolysaccharide-induced acute lung injury by upregulating Nrf2-dependent antioxidant responses, *Cell. Mol. Biol. Lett.*, 2022, **27**, 29.
52 C. Kim and B. Kim, Anti-cancer natural products and their bioactive compounds inducing ER stress-mediated apoptosis: A Review, *Nutrients*, 2018, **10**, 1021.
53 X. Xu, Y. Lai and Z. C. Hua, Apoptosis and apoptotic body: disease message and therapeutic target potentials, *Biosci. Rep.*, 2019, **39**, BSR20180992.
54 R. S. Wong, Apoptosis in cancer: from pathogenesis to treatment, *J. Exp. Clin. Cancer Res.*, 2011, **30**, 87.
55 D. Tewari, P. Patni, A. Bishayee, A. N. Sah and A. Bishayee, Natural products targeting the PI3K-Akt-mTOR signaling pathway in cancer: A novel therapeutic strategy, *Semin. Cancer Biol.*, 2022, **80**, 1–17.
56 X. Peng, X. Huan, T. B. Lulu, W. Jia, S. Zhang, L. Cohen, S. Huang, J. Fan, X. Chen, S. Liu, Y. Wang, K. Wang, S. Isoyama, S. Dan, F. Wang, Z. Zhang, M. Elkabets and D. Kong, A novel pan-PI3K inhibitor KTC1101 synergizes with anti-PD-1 therapy by targeting tumor suppression and immune activation, *Mol. Cancer*, 2024, **23**, 54.
57 J. Yang, J. Nie, X. Ma, Y. Wei, Y. Peng and X. Wei, Targeting PI3K in cancer: mechanisms and advances in clinical trials, *Mol. Cancer*, 2019, **18**, 26.
58 S. Revathidevi and A. K. Munirajan, Akt in cancer: Mediator and more, *Semin. Cancer Biol.*, 2019, **59**, 80–91.
59 L. Simonyan, T. T. Renault, M. J. Novais, M. J. Sousa, M. Côrte-Real, N. Camougrand, C. Gonzalez and S. Manon, Regulation of Bax/mitochondria interaction by AKT, *FEBS Lett.*, 2016, **590**, 13–21.
60 M. Shariati and F. Meric-Bernstam, Targeting AKT for cancer therapy, *Expert Opin. Invest. Drugs*, 2019, **28**, 977–988.
61 D. Mossmann, S. Park and M. N. Hall, mTOR signaling and cellular metabolism are mutual determinants in cancer, *Nat. Rev. Cancer*, 2018, **18**, 744–757.
62 H. Khan, A. Bangar, A. K. Grewal, P. Bansal and T. G. Singh, Caspase-mediated regulation of the distinct signaling pathways and mechanisms in neuronal survival, *Int. Immunopharmacol.*, 2022, **110**, 108951.
63 M. I. Avrutsky and C. M. Troy, Caspase-9: A multimodal therapeutic target with diverse cellular expression in human disease, *Front. Pharmacol.*, 2021, **12**, 701301.
64 A. Unnisa, N. H. Greig and M. A. Kamal, Inhibition of Caspase 3 and Caspase 9 Mediated Apoptosis: A Multimodal Therapeutic Target in Traumatic Brain Injury, *Curr. Neuropharmacol.*, 2023, **21**, 1001–1012.
65 X. Chen, J. Li, R. Kang, D. J. Klionsky and D. Tang, Ferroptosis: machinery and regulation, *Autophagy*, 2021, **17**, 2054–2081.
66 S. K. Georgiou-Siafis and A. S. Tsiftsoglou, The key role of GSH in keeping the redox balance in mammalian cells: mechanisms and significance of GSH in detoxification via formation of conjugates, *Antioxidants*, 2023, **12**, 1953.
67 B. Niu, K. Liao, Y. Zhou, T. Wen, G. Quan, X. Pan and C. Wu, Application of glutathione depletion in cancer therapy: Enhanced ROS-based therapy, ferroptosis, and chemotherapy, *Biomaterials*, 2021, **277**, 121110.
68 Y. Wu, J. Wang, T. Zhao, J. Chen, L. Kang, Y. Wei, L. Han, L. Shen, C. Long, S. Wu and G. Wei, Di-(2-ethylhexyl) phthalate exposure leads to ferroptosis via the HIF-1α/HO-1 signaling pathway in mouse testes, *J. Hazard. Mater.*, 2022, **426**, 127807.
69 G. P. Drummen, B. M. Gadella, J. A. Post and J. F. Brouwers, Mass spectrometric characterization of the oxidation of the fluorescent lipid peroxidation reporter molecule C11-BODIPY (581/591), *Free Radical Biol. Med.*, 2004, **36**, 1635–1644.
70 C. Chen, W. Chen, X. Zhou, Y. Li, X. Pan and X. Chen, Hyperbaric oxygen protects HT22 cells and PC12 cells from damage caused by oxygen-glucose deprivation/reperfusion via the inhibition of Nrf2/System Xc-/GPX4 axis-mediated ferroptosis, *PLoS One*, 2022, **17**, e0276083.
71 G. Miotto, M. Rossetto, M. L. Di, L. Orian, R. Venerando, A. Roveri, A. M. Vučković, V. Bosello, M. Zaccarin, L. Zennaro, M. Maiorino, S. Toppo, F. Ursini and G. Cozza, Insight into the mechanism of ferroptosis inhibition by ferrostatin-1, *Redox Biol.*, 2020, **28**, 101328.

72 T. M. Seibt, B. Proneth and M. Conrad, Role of GPX4 in ferroptosis and its pharmacological implication, *Free Radical Biol. Med.*, 2019, **133**, 144–152.
73 G. C. Forcina and S. J. Dixon, GPX4 at the crossroads of lipid homeostasis and ferroptosis, *Proteomics*, 2019, **19**, e1800311.
74 S. Sprouse, K. A. King, P. J. Spellane and R. J. Watts, Photophysical effects of metal-carbon σ bonds in ortho-metalated complexes of iridium(III) and rhodium(III), *J. Am. Chem. Soc.*, 1985, **106**, 6647–6653.
75 Y. D. Sarathkumara, D. J. Browne, A. M. Kelly, D. J. Pattinson, C. M. Rush, J. Warner, C. Proietti and D. L. Doolan, The Effect of tropical temperatures on the quality of RNA extracted from stabilized whole-blood samples, *Int. J. Mol. Sci.*, 2022, **23**, 10609.